

A Foundation Model for Virtual Sensors

Leon Götz^{1,2} Lars Frederik Peiss³ Erik Sauer³ Andreas Udo Sass¹ Thorsten Bagdonat¹
Stephan Günemann² Leo Schwinn²

Abstract

Virtual sensors use machine learning to predict target signals from available measurements, replacing expensive physical sensors in critical applications. Existing virtual sensor approaches require application-specific models with hand-selected inputs for each sensor, cannot leverage task synergies, and lack consistent benchmarks. At the same time, emerging time series foundation models are computationally expensive and limited to predicting their input signals, making them incompatible with virtual sensors. We introduce the first foundation model for virtual sensors addressing both limitations. Our unified model can simultaneously predict diverse virtual sensors exploiting synergies while maintaining computational efficiency. It learns relevant input signals for each virtual sensor, eliminating expert knowledge requirements while adding explainability. In our large-scale evaluation on a standard benchmark and an application-specific dataset with over 18 billion samples, our architecture achieves $415 \times$ reduction in computation time and $951 \times$ reduction in memory requirements, while maintaining or even improving predictive quality compared to baselines. Our model scales gracefully to hundreds of virtual sensors with nearly constant parameter count, enabling practical deployment in large-scale sensor networks.

1. Introduction

Many important applications in areas such as autonomous driving, environmental monitoring, and healthcare rely on high-quality sensors. Unfortunately, these sensors can be expensive, difficult to maintain, or unsuitable for large-scale deployment. Virtual sensors address this limitation by computing target signals from available other measurements

¹Volkswagen AG ²Department of Computer Science & Munich Data Science Institute Technical University of Munich ³Work done during an internship at Volkswagen AG. Correspondence to: Leon Götz <leon.goetz@volkswagen.de>.

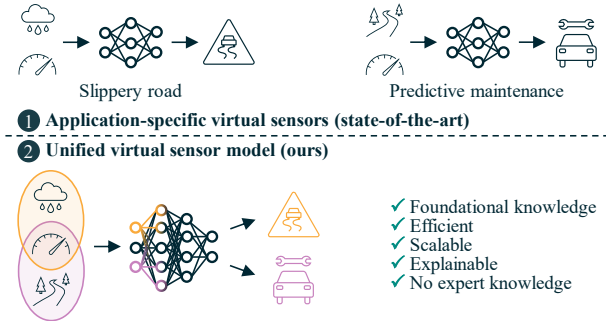


Figure 1. ① Recent works train, maintain, and deploy isolated application-specific models for every virtual sensor. ② Our foundational approach unifies multiple virtual sensors into a single model, exploiting synergies and achieving superior scalability. It learns relevant input signals and selectively predicts virtual sensors, increasing efficiency and explainability without expert knowledge.

through statistical or learning-based methods (Albertos & Goodwin, 2002). They can replace physical sensors, saving costs, act as redundancy in safety-critical applications, allow for non-invasive measurements, or compute quantities that are not measurable with physical sensors, such as a battery’s state of health (von Bülow et al., 2021).

While some deep learning-based approaches exist for virtual sensor simulation, they exhibit four key limitations. First, they rely on highly application-specific models that are trained, deployed, and maintained separately for each virtual sensor, with input signals typically being hand-selected by domain experts (Ziaukas et al., 2021). As a result, current approaches do not scale to large sensor networks. Second, these isolated models cannot leverage synergies among different virtual sensor tasks, requiring one individual model for every simulated sensor. Third, there is little consistency in how virtual sensors are evaluated, with few works using standard benchmark datasets (Hu et al., 2024). Lastly, existing methods tend to rely on relatively simple deep learning models (Dos Santos Diniz et al., 2025), potentially limiting their performance.

Recently, foundation models have shown impressive performance in time series forecasting, outperforming specialized approaches (Ansari et al., 2024). These unified models exploit synergies among different tasks and datasets. However, large foundation models impose considerable computation requirements (Götz et al., 2025), limiting their application in

sensor networks with thousands of signals (Godahewa et al., 2021). Additionally, current time series foundation models only forecast the input signals and cannot predict new signals, making them unsuitable for virtual sensor tasks.

We address these complementary gaps through a unified foundation model for virtual sensors. By training a single model across multiple virtual sensor tasks, we overcome the scalability and synergy limitations of existing virtual sensor approaches. Simultaneously, we design our architecture to be computationally efficient, addressing the deployment constraints that prevent current foundation models from being applied to large-scale sensor networks with thousands of signals. Our key contributions are:

Large-scale benchmark We provide the first large-scale analysis of unified virtual sensor models on a common time series forecasting benchmark and an application-specific automotive dataset with over 17 500 km of driving and 18 B time series samples using over 43 500 H100 GPU hours.

Foundation model for virtual sensors Our unified model can predict multiple virtual sensors. By exploiting synergies among them and leveraging foundational time series knowledge, it scales gracefully to large sensor networks while even improving predictive quality in some cases. We demonstrate that our approach learns the set of relevant input signals for each virtual sensor, thereby adding explainability and eliminating the need for expert knowledge in virtual sensor design. Due to its flexible sensor selection mechanism, it achieves high efficiency, making it suitable for on-device computing.

Results Our evaluation on a standard benchmark and an application-specific automotive dataset reveals substantial computational savings with minimal impact on predictive quality. Our model reduces computation time up to $415 \times$ and minimizes memory requirements by $951 \times$ compared to standard approaches. It scales to hundreds of virtual sensors with an almost constant number of trainable parameters.

2. Related work

In this work, we design a foundation model for virtual sensor applications, aligning two previously disjoint literature branches for application-specific virtual sensors and foundation models for time series forecasting.

Virtual sensors Virtual sensors offer practical advantages by reducing costs, improving reliability, enabling non-invasive measurements, and estimating quantities not directly measurable with physical sensors. In the automotive domain, virtual sensors improve safety by estimating dynamic parameters such as the side slip angle (Ziaukas et al., 2021; Kalyanasundaram et al., 2025), compute environmentally relevant nitrogen oxide emissions (Arsie et al., 2017),

or estimate battery temperatures (Bamati et al., 2024), or a battery’s state of health (von Bülow et al., 2021). Virtual sensors are also used in the mining domain to determine mass flow rates of ore from electrical conveyor belt currents (Dos Santos Diniz et al., 2025), in food production to estimate moisture contents (Wang et al., 2001), in chemical processes to discriminate between different gases (Ankara et al., 2004), or in healthcare to measure blood pressure non-invasively (Attivissimo et al., 2023) or detect heart disease from the patient’s breath (Hu et al., 2024). While early works on virtual sensors mostly utilize hand-crafted models (Albertos & Goodwin, 2002), current literature predominantly identifies models from data using simple machine learning techniques (Dos Santos Diniz et al., 2025). However, the set of input signals for virtual sensors is still an expert choice and models are designed highly application-specific for every virtual sensor task. This severely limits the scalability and prevents leveraging synergies among different virtual sensor tasks due to isolated models. Further, as virtual sensors are highly application-driven, the literature lacks consistent evaluation on widely used benchmark datasets.

Time series foundation models Recently, foundation models have emerged, forecasting univariate (Das et al., 2023b; Ansari et al., 2024; Rasul et al., 2023; Goswami et al., 2024; Liu et al., 2024b; 2025; Auer et al., 2025b) or multivariate time series (Woo et al., 2024; Gao et al., 2024; Cohen et al., 2024; Ekambaram et al., 2024), sometimes with additional covariates (Das et al., 2023a; Wang et al., 2024; Auer et al., 2025a; Patil et al., 2025; Ansari et al., 2025). These models have shown impressive forecasting performance and generalization capability, outperforming specialized approaches (Ansari et al., 2024). However, large foundation models impose considerable computation requirements, constraining their applicability in sensor networks and on edge devices (Götz et al., 2025). Further, current time series foundation models are only able to forecast signals for which they have past context and cannot generalize to predict new signals from other measurements, making them incompatible with virtual sensor tasks. Building on the assumption of self-contained time series (Chen et al., 2025), some approaches limit cross-signal interactions to reduce model complexity, often utilizing proxy measures for signal importance such as the correlation (Lee et al., 2024; Chen et al., 2024; Liu et al., 2024a; Qiu et al., 2025; Hu et al., 2025). However, these methods do not realize efficiency improvements in practice, as the unstructured sparsity they induce cannot be exploited by standard hardware for computational speedup.

We propose a unified foundation model for multiple virtual sensors within a sensor network that leverages cross-task synergies while maintaining computational efficiency. It learns the set of relevant input signals, minimizing expert knowledge requirements and enhancing explainability.

3. A foundation model for virtual sensors

We design a unified foundation model exploiting synergies among multiple virtual sensors. After introducing our basic model architecture, we propose a novel mechanism to selectively predict new signals that are not in the input set. We then design a mechanism to learn the set of relevant input signals per virtual sensor, minimizing expert knowledge, enhancing explainability, and improving efficiency. Finally, we introduce efficient training methods.

Let $\mathcal{Z} = \{z_i\}_{i=1}^M$ be a family of univariate real-valued time series (input signals) index by $i = 1, \dots, M$ and $\mathcal{Z}' = \{z'_j\}_{j=1}^N$ be another family of univariate real-valued time series (virtual sensors) index by $j = 1, \dots, N$, where \mathcal{Z} and \mathcal{Z}' are typically disjoint but can also be overlapping, or identical. Let a neural network $\mathbf{f}_\theta(\mathbf{x}) = \Phi_L \circ \Phi_{L-1} \circ \dots \circ \Phi_1(\mathbf{x})$ with parameters θ consist of L layers denoted as Φ_l , where each layer takes the output of the previous layer as input. Based on a model \mathbf{f}_θ , we predict N virtual sensors \mathcal{Z}' from M input time series \mathcal{Z} . We assume that the neural network's input $\mathbf{x} \in \mathbb{R}^{s \times d}$ consists of s tokens with dimension d . Here, the input tokens are generated by a tokenizer \mathbf{g} out of input data \mathcal{Z} .

3.1. Base architecture

Based on the competitive results in Das et al. (2023b), we use a causal decoder-only transformer as the base architecture for our model \mathbf{f}_θ . We tokenize our input time series $z_i \in \mathcal{Z}$ individually. To this end, we first normalize each series to have zero mean and unit standard deviation and extract non-overlapping patches of length p in a second step (Nie et al., 2023). Subsequently, we embed each patch into the token dimension d using a multi-layer perceptron $\mathbb{R}^p \rightarrow \mathbb{R}^d$ (Das et al., 2023b). Finally, our tokenizer \mathbf{g} concatenates all tokens into a single token sequence $\mathbf{x} \in \mathbb{R}^{s \times d}$ with time-based ordering as in figure 2. We follow a similar approach when de-embedding predicted tokens back to time series representations.

3.2. Selective prediction of virtual sensors

We embed temporal and variate information into our token sequence using sin-cos (Vaswani et al., 2017) and learned position embedding, respectively. While current time series literature that forecasts only input signals omits variate information (Woo et al., 2024; Ansari et al., 2025), embedding it explicitly is crucial for our proposed mechanism to predict virtual sensors. The temporal position embedding is shared among variates, while the variate embedding is shared orthogonally across time. We learn additive variate embedding vectors $\mathcal{V} = \{v_i\}_{i=1}^M$ for input signals $z_i \in \mathcal{Z}$ and $\mathcal{V}' = \{v'_j\}_{j=1}^N$ for virtual sensors $z'_j \in \mathcal{Z}'$, with $v_i, v'_j \in \mathbb{R}^d$.

We design a novel mechanism to forecast new signals (virtual sensors) autoregressively in a selective way. To predict the j -th virtual sensor from the input signals \mathcal{Z} , we insert a zero-vector $\vec{0}$ as an initially empty prototype token into our token sequence \mathbf{x} (see figure 2). Subsequently, the additive time and variate embedding v'_j allows the neural network to learn the mapping of relevant target information into the prototype token. We train our model $\mathbf{f}_\theta(\mathbf{x})$ to forecast the next p time steps of our virtual sensor j into the future. For the following autoregressive steps, we leverage our model's previous prediction as new input for virtual sensor signals z'_j . This way, our model starts autoregressive generation from an empty prototype token in the first step and only needs to predict residuals from increasing context in the following. For input signals \mathcal{Z} , we use ground truth measurements in all autoregressive steps. This setup mimics practical deployment scenarios where ground truth measurements from physical input sensors are available, but virtual sensor outputs must be predicted autoregressively. To forecast multiple virtual sensors in a single step, we simply add multiple prototype tokens with their respective position embeddings to the network's input. Our approach enables flexible selection of which virtual sensors to predict in each generation step, ranging from a single sensor to all sensors simultaneously. This capability addresses two practical requirements in sensor networks. First, different signals are often needed at different frequencies; for example, a vehicle's engine temperature requires higher update rates than ambient temperature due to faster control cycles. Second, by forecasting into the future, our model compensates for its own inference latency and enables predictive functionalities such as early fault detection (Albertos & Goodwin, 2002).

3.3. Learning relevant input signals

In classical virtual sensor literature, the set of input signals \mathcal{Z} is chosen by experts. However, in large sensor networks, this can be challenging and prone to error. To address this, we end-to-end learn the set of relevant input signals for each virtual sensor, minimizing expert knowledge and enhancing explainability and efficiency. To this end, we introduce signal relevance vectors $\mathcal{R}' = \{r'_j\}_{j=1}^N$ with $r'_j \in \mathbb{R}^{M+N}$ for every virtual sensor j . Each vector r'_j encodes the relevance of all available sensors, both input signals and other virtual sensors, for predicting virtual sensor j , enabling hierarchical dependencies among virtual sensors. When predicting a virtual sensor, we select the corresponding relevance vector r'_j and compute the cross-relevance for the communication of signal pairs using the outer product $(r'_j \cdot r'^T_j) \in \mathbb{R}^{(M+N) \times (M+N)}$. We then duplicate our relevance matrix across time (see figure 2), as we aim to learn global time-independent signal relevance. Finally, we apply this matrix B in the attention score computation (Vaswani et al., 2017) of every transformer layer l as static bias in

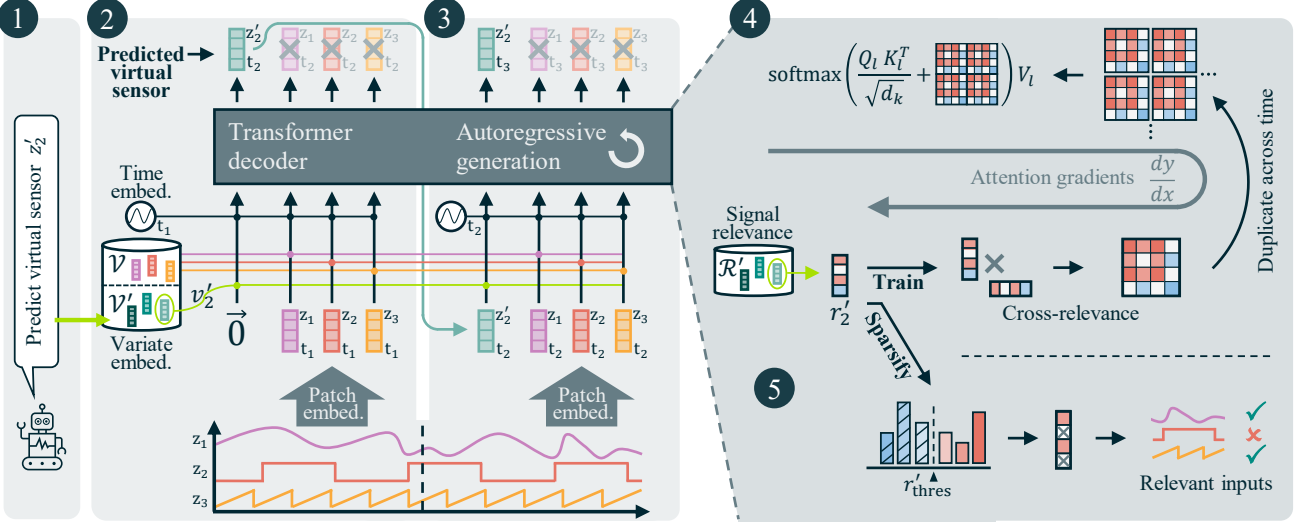


Figure 2. We present a foundation model that can predict a user-selected target virtual sensor (z'_2 , green) out of multiple possible virtual sensors. ① We first define which virtual sensor to forecast (here sensor z'_2). ② Next, we introduce an initially empty prototype token $\vec{0}$ and add the corresponding variate embedding $v'_2 \in \mathcal{V}'$ to guide the neural network to predict the specified virtual sensor, based on available sensor signals (z_1 , pink; z_2 , red; z_3 , orange). We divide input signals z_1, z_2, z_3 into patches, embed them into tokens, and add time and variate embedding \mathcal{V} to them. Starting from empty prototypes in cycle t_1 , ③ we forecast virtual sensors autoregressively using the model’s previous prediction z'_2 as current input in step t_2 . ④ Within the transformer, our architecture learns relevant input signals for each virtual sensor from attention gradients through trainable signal relevance vectors \mathcal{R}' , adding explainability. After selecting the corresponding signal relevance vector r'_2 , we compute the cross-relevance for signal-to-signal communication, duplicate our mask across time to learn time-independent signal importance, and apply it as attention bias. ⑤ By later sparsifying signal relevance vectors \mathcal{R}' based on a threshold r'_{thres} , we structurally prune irrelevant input signals to achieve considerable efficiency gains.

equation (1). At the beginning of training, we initialize our relevance vectors \mathcal{R}' with ones, as zero vectors would prevent gradient flow, utilizing the translation invariance of the softmax function.

$$\text{Attention}(Q, K, V)_l = \text{softmax} \left(\frac{Q_l K_l^T}{\sqrt{d_k}} + B \right) V_l \quad (1)$$

While current work determines signal importance using proxy measures such as correlation at the time series level (Lee et al., 2024), we directly learn relevance by backpropagating gradients from attention score computation to our relevance vectors \mathcal{R}' . As we share our mask across transformer layers, signal relevance is determined based on simple features in the first layers, but can leverage more complex representations in deeper layers.

Efficient processing via sparsification To increase the efficiency of our foundation model and enable applications on edge devices, we sparsify our relevance vectors $r'_j \in \mathcal{R}'$ at late training stages and inference time. To this end we mask unimportant signals in r'_j with $-\infty$ based on a threshold r'_{thres} , which controls the sparsity of the attention map and which signals are used for forecasting. Our masking is equivalent to completely disregarding unimportant signals as the outer product operation and duplication across time generate fully masked rows and columns in our attention bias B in a structured way. This enables us to learn individual input signal sets $\{\mathcal{Z}_j \subseteq \mathcal{Z}\}_{j=1}^N$ for every virtual sensor.

Together with our virtual sensor selection mechanism in section 3.2, we achieve maximum efficiency by querying our model only for currently requested virtual sensors and using only relevant input signals for these sensors. This reduces the number of tokens s to be processed to a minimum. When requesting multiple virtual sensors simultaneously, we simply average the corresponding attention biases B and union the individual input signal sets.

3.4. Efficient training strategies

We optimize the parameters $\theta \in \Theta$ of our model f_θ to minimize the mean squared error only of virtual sensor forecasts. Predicted input signals are not included in loss computation (see figure 2). Training all virtual sensors $z'_j \in \mathcal{Z}'$ simultaneously in every training step, however, is impractical as all signal relevance vectors $r'_j \in \mathcal{R}'$ would be updated with identical gradients, resulting in identical input sets $\mathcal{Z}_j \subseteq \mathcal{Z}$ for all sensors¹. Training a single virtual sensor at a time, instead, is inefficient, prolonging the training process due to less informative gradients. As a consequence, we select a random subset of $N_{\text{train}} < N$ virtual sensors in every training iteration. Similar to dropout (Srivastava et al., 2014), this reduces the correlation among relevance vectors.

¹Adding random noise mitigates identical gradients but cannot ensure the correct mapping of input signals to virtual sensors.

Teacher forcing Our model generates virtual sensor predictions autoregressively as described in [section 3.2](#). Standard training via backpropagation through time ([Rumelhart et al., 1985](#)) would incur high memory and computational costs due to long recurrent gradient paths and multiple forward passes per training step. Thus, we employ teacher forcing ([Williams & Zipser, 1989](#)), removing the recurrent path in [figure 2](#), and use ground truth data for virtual sensors during training. This enables simultaneous training on multiple context lengths with a single model iteration, yielding short gradient paths and fast training cycles. However, teacher forcing limits the model’s ability to learn error propagation strategies. To mitigate this, we explore hybrid training schedules that combine teacher forcing with fine-tuning via backpropagation through time in [section 5.6](#).

4. Experiments

We systematically train and evaluate our foundation model on 16 virtual sensor tasks and 2 datasets, demonstrating performance and efficiency gains of our unified architecture. In [appendix A](#), we provide further experimental details.

Datasets For our experiments, we utilize Traffic as a standard time series forecasting dataset and a CAN bus vehicle dataset for application-specific evaluation. Traffic consists of 862 identical sensors measuring the hourly road occupancy in the San Francisco Bay Area and contains roughly 15 M time series samples ([Godahewa et al., 2021](#)). It shares a similar periodic structure among variates as in [figure 7](#). The CAN bus (controller area network bus) enables communication between electronic control units in vehicles ([ISO 11898, 1993](#)). To evaluate our architecture in a realistic deployment setting, we use a large-scale proprietary CAN bus dataset with 1713 variates including continuous sensor measurements, categorical states, and event-based signals. It features substantially more complex signal interactions than the Traffic dataset, e.g., the categorical driving mode (eco, sport, comfort, ...) influences pedal curves, stability, power delivery, efficiency, and generally driving behavior. Our CAN bus dataset is recorded with an Audi e-tron electric vehicle covering 287 hours of driving and over 17 500 km on German roads. It is synchronized to 100 ms granularity and is substantially larger than Traffic with approximately 18 B time series samples.

Virtual sensors For the Traffic dataset, we randomly select our set \mathcal{Z}' of $N = 16$ virtual sensors, as all variates present the same quantity, measured at different locations. In the CAN bus dataset, every signal has a distinct purpose. Here, we hand-pick $N = 16$ virtual sensors with clear intuitive interpretations, including electrical powertrain voltages, currents, and temperatures, coolant intake and outflow temperatures and flow-rates, torques and velocities.

Models Throughout our experiments we train and evaluate models with $L = 4$ transformer layers, 4 heads, and token dimension $d = 512$. All our models and baselines have similar capacity with 7.4 M trainable parameters for Traffic and 7.8 M for the CAN bus dataset, due to different numbers of learned variate embedding vectors \mathcal{V} . The signal relevance vectors \mathcal{R}' account for only 13.8 k and 27.4 k parameters, respectively. We utilize patches with length $p = 32$ to divide time series into tokens. For evaluation, we perform 6 autoregressive generation cycles.

5. Results

The overarching goal of our experiments is to investigate the feasibility of a unified virtual sensor foundation model. First, we demonstrate efficiency and superior scaling properties ([sec. 5.1](#)). In particular, we investigate efficiency gains through focusing only on relevant input signals ([sec. 5.2](#)) and through flexibly predicting a subset of virtual sensors ([sec. 5.3](#)). We then explore the scaling of our unified model to hundreds of virtual sensors ([sec. 5.4](#)) and highlight explainability benefits of our architecture ([sec. 5.5](#)). Finally, we investigate efficient training techniques ([sec. 5.6](#)).

5.1. Main experiments

The application-specific nature of virtual sensor methods has resulted in a lack of consistent benchmarks. Meanwhile, time series foundation models cannot predict new, unseen signals from other measurements, limiting their applicability to virtual sensor tasks. We address both gaps through two contributions. First, we establish a baseline on a standardized benchmark. Here, we train an individual model for every sensor as done in prior work ([Ziaukas et al., 2021](#)). Second, we introduce a unified baseline that predicts all virtual sensors from available input signals at every step and systematically introduce and ablate novel components that enable the training and deployment of a large-scale foundation model: (i) variate embeddings, (ii) learned relevance masking, (iii) sparsification, and (iv) sensor selection.

As a baseline, we train 16 isolated models to predict a single virtual sensor each. On the Traffic dataset, classical virtual sensors achieve marginally better MSE, while our unified approach outperforms isolated models substantially on CAN bus data. We hypothesize that exploiting synergies using our foundation model is more important in complex sensor networks with related virtual sensor tasks, such as the CAN bus, compared to Traffic, where every sensor is similar. Relying on foundational time series understanding, our unified approach scales superior compared to training, maintaining, and deploying 16 isolated models with in total $16 \times$ the number of parameters, which we further investigate in [section 5.4](#). (i) Our results in [table 1](#) demonstrate that variate embeddings are crucial for predicting virtual sensors.

Table 1. Comparison of a simple **unified model** predicting all 16 virtual sensors, where we subsequently introduce our proposed mechanisms, with 16 **individual models** predicting a single virtual sensor each. We list MSE, inference time, dynamic CUDA peak memory, and the number of trainable parameters for Traffic and CAN bus datasets.

Architecture	Traffic				CAN bus			
	MSE	Time	Mem.	Param.	MSE	Time	Mem.	Param.
Individual models								
+ Variate embedding $\mathcal{V}, \mathcal{V}'$	0.251	16.62 ms	0.90 GB	118.4 M	0.177	58.05 ms	3.42 GB	124.8 M
Unified model	0.556	16.70 ms	0.90 GB	7.0 M	0.727	58.19 ms	3.46 GB	7.0 M
+ Variate embedding $\mathcal{V}, \mathcal{V}'$	0.275	16.76 ms	0.90 GB	7.4 M	0.119	58.23 ms	3.46 GB	7.8 M
+ Signal relevance \mathcal{R}'	0.272	16.85 ms	0.90 GB	7.4 M	0.136	58.41 ms	3.46 GB	7.8 M
+ $N_{\text{train}} = 4$								
+ Sparse input sets \mathcal{Z}_j	0.282	0.87 ms	0.0352 GB	7.4 M	0.121	0.14 ms	0.0036 GB	7.8 M
+ Sensor selection								

This is contrary to current time series forecasting literature that can only predict input signals (Woo et al., 2024; Ansari et al., 2025). (ii) Further, introducing signal relevance vectors and training only a subset of virtual sensors per iteration $N_{\text{train}}/N = 4/16$ adds explainability and does not significantly affect predictive quality or efficiency. (iii) Additionally, we sparsify our learned signal relevance to determine individual input signal subsets $\mathcal{Z}_j \subseteq \mathcal{Z}$ for each virtual sensor. (iv) Together with our sensor selection mechanism, where we flexibly query our model to predict only currently required virtual sensors, we achieve high efficiency gains. Remarkably, we improve inference time by $415 \times$ and reduce memory requirements by $951 \times$ without affecting MSE on the CAN bus dataset. This enables our foundation model to run on edge devices in large sensor networks.

5.2. Different MSE efficiency trade-offs for variable test-time computation

To distinguish between important input signals $\mathcal{Z}_j \subseteq \mathcal{Z}$ and unimportant ones for each virtual sensor, we threshold our signal relevance vectors $r'_j \in \mathcal{R}'$ with r'_{thres} . Varying this threshold, we achieve different trade-offs between predictive quality and efficiency. Sparsification towards the end of training allows the model to adapt to reduced input sets, while sparsification only during inference might be more flexible. To compare both approaches, we train models with different sparsity thresholds.

Our results in figure 3 show that we can achieve high input sparsity without affecting predictive quality as most input signals are unimportant for individual virtual sensor tasks. Towards very high sparsity, MSE increases as we now also remove informative signals from the input sets. The approach is highly flexible in practice, as sparsification can be applied solely at inference time with minimal performance degradation. On the Traffic dataset, models trained with sparse inputs achieve only marginal improvements over inference-time sparsification. Moreover, on CAN bus data, both sparsification approaches exhibit similar performance

(see appendix B.1). This allows inference-time sparsification to flexibly adapt to varying computational budgets for each prediction, without requiring the loading of different model checkpoints. Only the set of input signals is dynamically adjusted. This is particularly relevant in real-world applications where computational resources may be limited during critical situations, or where faster inference is required to ensure timely decision-making.

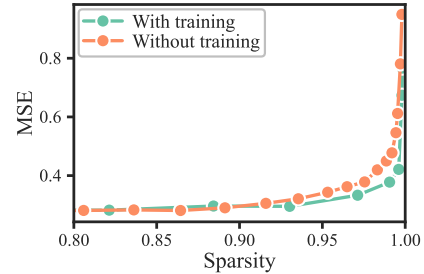


Figure 3. Varying our signal importance threshold r'_{thres} during training or inference generates smooth trade-offs between input set sparsity and MSE on the Traffic dataset.

5.3. Sensor selection maximizes efficiency without affecting predictive quality

In practical applications, virtual sensors are often required at varying frequencies. For example, engine-related measurements typically demand higher sampling rates than ambient signals in vehicles. Moreover, different virtual sensors generally rely on distinct sets of relevant input signals. To predict multiple virtual sensors simultaneously, we union their respective input signal sets, reducing sparsity. In the limiting case of equally sized, disjoint input sets, sparsity decreases linearly with the number of predicted virtual sensors. To address this, we introduce a sensor selection mechanism that enables the model to predict only the virtual sensors currently required, ensuring maximum efficiency when a specific signal is requested. In the following, we demonstrate the effectiveness of our approach by predicting an increasing number of virtual sensors simultaneously.

By selectively predicting subsets of virtual sensors—ranging from all sensors to individual sensors—per autoregressive step, we increase sparsity from 58.4 % to 81.9 % on the Traffic dataset (see [figure 4](#)). This translates to an additional $4.8 \times$ inference acceleration and $4.6 \times$ memory reduction. For CAN bus data efficiency gains are even higher with $7.9 \times$ and $13.4 \times$, respectively (see [appendix B.2](#)). As more virtual sensors are predicted simultaneously, sparsity decreases sub-linearly since related sensors often share common input signals. The number of simultaneously predicted signals does not affect predictive quality in our experiments.

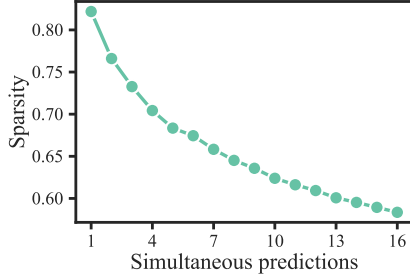


Figure 4. Sparsity increases as fewer virtual sensors are predicted simultaneously through our sensor selection mechanism. Results are shown for the Traffic dataset.

5.4. Scaling to hundreds of virtual sensors

Classical approaches train a single model for each virtual sensor. As the number of virtual sensors grows, this causes a linear increase in training and deployment effort and model parameters, making it impractical at scale. In contrast, our unified model maintains an almost constant number of trainable parameters when scaling to large sensor networks. However, modeling capacity might be a limitation for our fixed-size neural network. To investigate this, we train models to predict increasing numbers of virtual sensors $N_{\text{Traffic}} \in \{4, 8, 16, \dots, 512\}$, $N_{\text{CAN}} \in \{4, 8, 12, 16\}$ and evaluate them on a constant set of 4 core sensors.

As the number of learned virtual sensors increases, predictive quality of our models remains stable with a standard deviation of 0.028 on Traffic and 0.008 on the CAN bus dataset. This experiment demonstrates that our foundation model possesses sufficient capacity to learn hundreds of virtual sensors. We argue that our architecture scales gracefully by leveraging shared knowledge across virtual sensors.

5.5. Explainability of virtual sensors

Beyond substantial efficiency improvements, learning the relevant input signal sets for each virtual sensor enhances explainability, which is particularly important in safety-critical applications. Furthermore, it allows for robustness analysis to identify which virtual sensors remain functional under conditions of incomplete input availability. Here, we investigate the learned signal relevance in detail.

Qualitative assessment We utilize expert knowledge to analyze the learned input signal sets for the individual virtual sensors. For this purpose, we use the CAN bus dataset, as every virtual sensor can be associated with an interpretable physical quantity. We find that our relevance vectors learn meaningful selections. Virtual sensors for temperatures mainly rely on other temperatures together with coolant flow rates, while virtual sensors for torques utilize engine speeds, velocities, and acceleration signals. Sensors for electrical voltages, in contrast, rely mostly on other voltages and electrical current signals as we visualize in [appendix B.4](#). This facilitates the benefit of learning individual input sets for every virtual sensor. Overall, the input sets align well with domain expert assessments, confirming their plausibility.

Quantitative assessment We learn input signal relevance through attention gradients. Here, we compare our approach to choosing input signals randomly or utilizing signal correlations between inputs and virtual sensors as a proxy metric. For a fixed sparsity, our approach substantially outperforms random and correlation-based input signal sets as our results in [table 2](#) show. We argue that learning relevant signals directly through attention gradients exploits both semantically simple features and complex ones in deeper neural network layers. In contrast, correlation as a proxy only relies on simple time series features, which may represent a considerable limitation for complex sensor networks, such as the CAN bus.

Table 2. Comparison of different methods to determine signal relevance on the Traffic and the CAN bus dataset. **Best** in bold.

Signal relevance	Traffic		CAN bus	
	Sparsity	MSE	Sparsity	MSE
Random	0.820	0.319	0.977	0.601
Correlation	0.820	0.492	0.978	0.267
Learned	0.821	0.282	0.978	0.121

Synthetic data Our model learns to identify input signals based on their variate embedding, to attribute importance scores to them through signal relevance vectors, and to compute the right virtual sensor according to our sensor selection mechanism. Here, we validate the seamless interplay of these three mechanisms, leveraging synthetic data. To this end, we generate a dataset with $M = 1000$ random, uncorrelated signals. We train a model to replicate $N = 2$ input signals z_{100}, z_{200} as virtual sensors z'_1, z'_2 , respectively. Throughout the learning process, our model subsequently identifies both input signals (see [figure 5](#)). It attributes at least $4.22 \times$ higher relevance to them compared to all other 998 signals. Finally, it selects the correct signal as virtual sensor output. This experiment demonstrates the seamless interaction of identification, relevance, and selection mechanisms in our architecture.

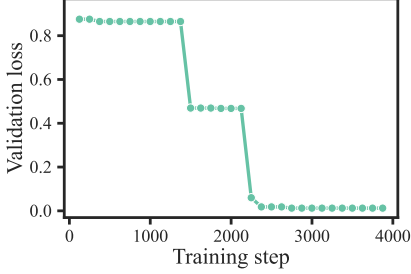


Figure 5. Our architecture subsequently identifies 2 virtual sensors among 1000 signals in our synthetic random dataset during training, reducing the validation loss in a stepwise manner.

5.6. Efficient training strategies

Training virtual sensors simultaneously Learning multiple virtual sensors per training iteration improves training efficiency. However, training all virtual sensors in every cycle ultimately results in identical signal relevance vectors, as they receive identical gradients and therefore identical input signal sets for all virtual sensors. We explore this trade-off in detail by training models with $N_{\text{train}} \in \{1, 2, 3, 4, 6, 8, 10, 13, 16\}$ and measure the average similarity of the sensors’ input signal sets $\mathcal{Z}_j \subseteq \mathcal{Z}$. Training a single virtual sensor at a time results in most specialized input sets that share 12.7 % of the signals on average as in figure 6. However, training generally requires more iterations due to less informative gradients. In contrast, learning multiple virtual sensors simultaneously results in more similar input signal sets, but makes training more efficient. In practice, we find $N_{\text{train}} = 4$ to be a good tradeoff between training time and input set separation. We show results for the CAN bus dataset in appendix B.3 and provide additional analysis in appendix B.5.

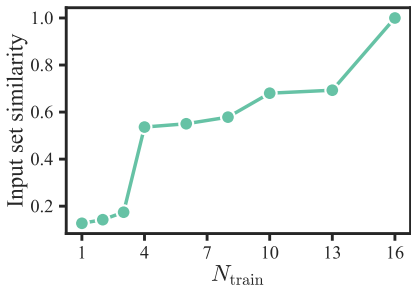


Figure 6. Learning different numbers of virtual sensors N_{train} in a single training iteration influences the similarity of their input signal sets on the Traffic dataset.

Teacher forcing Our model generates virtual sensor predictions autoregressively during inference. For training, however, we utilize teacher forcing as a more efficient strategy. Compared to backpropagation through time, teacher forcing requires only a single model forward pass, substantially reducing memory usage and training time. However, this approach prevents the model from learning to correct for

accumulated errors during inference. We compare teacher forcing and backpropagation through time training strategies in the following.

Even with extensive hyperparameter tuning, training with backpropagation through time diverges. We argue that this is due to long recurrent gradient paths. Conversely, training with teacher forcing converges smoothly, while being $5.8 \times$ faster and consuming $4.3 \times$ less memory, as shown in table 3. Throughout our paper, the low inference MSE indicates that models trained with teacher forcing successfully predict initial tokens from empty prototypes, as well as subsequent tokens, and do not suffer from extensive error accumulation in autoregressive forecasting. We do not find a significant difference when comparing the predictive loss of initial tokens to that of subsequent ones. We provide further evidence for the effectiveness of teacher forcing in appendix B.7. Additionally, we experiment with backpropagation through time as a fine-tuning step starting from a teacher-forcing checkpoint. This hybrid schedule allows us to maintain efficient training for most of the process while explicitly introducing error propagation toward the end of training. Table 3 shows that this approach further improves predictive performance.

Table 3. Comparison of teacher forcing, back propagation through time (BPTT), and a combination of both for training our model on the CAN bus dataset. We list MSE, time per training iteration, and dynamic CUDA peak memory. **Best** in bold.

Training strategy	MSE	Time	Mem.
Teacher forcing	0.136	0.19 s	16.6 GB
BPTT	X	1.11 s	72.0 GB
BPTT fine tuning	0.083	1.10 s	72.0 GB

6. Conclusion

In this work, we present the first foundation model for virtual sensors. Our architecture simultaneously predicts variable sensor subsets, exploiting task synergies while focusing only on relevant input signals to ensure both explainability and efficiency. In our large-scale evaluation on standard and application-specific datasets with billions of samples, we demonstrate substantial efficiency gains, flexible test-time computation trade-offs, and scalability to hundreds of virtual sensors. This enables practical deployment in large sensor networks and on resource-constrained devices. We hope our foundation model unlocks new virtual sensor applications and contributes to more environmentally sustainable time series modeling.

Limitations In our work, we do not conduct hyperparameter search for all possible parameters due to the high cost of training large foundation models. We expect even better results with optimized settings.

Impact statement

We propose a unified foundation model for virtual sensors and demonstrate its efficiency and scalability. We hope it enables new large-scale virtual sensor deployments to complement physical sensor networks, while reducing the environmental impact, resource consumption, and cost.

Disclaimer The results, opinions, and conclusions expressed in this publication are not necessarily those of Volkswagen Aktiengesellschaft.

References

Albertos, P. and Goodwin, G. C. Virtual sensors for control applications. In *Annual Reviews in Control*, 2002.

Ankara, Z., Kammerer, T., Gramm, A., and Schütze, A. Low power virtual sensor array based on a micromachined gas sensor for fast discrimination between h₂, co and relative humidity. In *Sensors and Actuators B: Chemical*, 2004.

Ansari, A. F., Stella, L., Turkmen, C., Zhang, X., Mercado, P., Shen, H., Shchur, O., Rangapuram, S. S., Arango, S. P., Kapoor, S., Zschiegner, J., Maddix, D. C., Wang, H., Mahoney, M. W., Torkkola, K., Wilson, A. G., Bohlke-Schneider, M., and Wang, Y. Chronos: Learning the language of time series. In *Transactions on Machine Learning Research*, 2024.

Ansari, A. F., Shchur, O., Küken, J., Auer, A., Han, B., Mercado, P., Rangapuram, S. S., Shen, H., Stella, L., Zhang, X., Goswami, M., Kapoor, S., Maddix, D. C., Guerzon, P., Hu, T., Yin, J., Erickson, N., Desai, P. M., Wang, H., Rangwala, H., Karypis, G., Wang, Y., and Bohlke-Schneider, M. Chronos-2: From univariate to universal forecasting. *arXiv:2510.15821*, 2025.

Arsie, I., Cricchio, A., De Cesare, M., Lazzarini, F., Pianese, C., and Sorrentino, M. Neural network models for virtual sensing of nox emissions in automotive diesel engines with least square-based adaptation. In *Control Engineering Practice*, 2017.

Attivissimo, F., D'Alessandro, V. I., De Palma, L., Lanzolla, A. M. L., and Di Nisio, A. Non-invasive blood pressure sensing via machine learning. In *Sensors*, 2023.

Auer, A., Parthipan, R., Mercado, P., Ansari, A. F., Stella, L., Wang, B., Bohlke-Schneider, M., and Rangapuram, S. S. Zero-shot time series forecasting with covariates via in-context learning. *arXiv:2506.03128*, 2025a.

Auer, A., Podest, P., Klotz, D., Böck, S., Klambauer, G., and Hochreiter, S. Tirex: Zero-shot forecasting across long and short horizons with enhanced in-context learning. *arXiv:2505.23719*, 2025b.

Bamati, S., Chaoui, H., and Gualous, H. Enhancing battery thermal management with virtual temperature sensor using hybrid cnn-lstm. In *IEEE Transactions on Transportation Electrification*, 2024.

Chen, J., Lenssen, J. E., Feng, A., Hu, W., Fey, M., Tassiulas, L., Leskovec, J., and Ying, R. From similarity to superiority: Channel clustering for time series forecasting. In *Advances in Neural Information Processing Systems*, 2024.

Chen, Y., Céspedes, N., and Barnaghi, P. A closer look at transformers for time series forecasting: Understanding why they work and where they struggle. In *International Conference on Machine Learning*, 2025.

Cohen, B., Khwaja, E., Wang, K., Masson, C., Ramé, E., Doublé, Y., and Abou-Amal, O. Toto: Time series optimized transformer for observability. *arXiv:2407.07874*, 2024.

Cowen-Rivers, A., Lyu, W., Tutunov, R., Wang, Z., Grosnit, A., Griffiths, R.-R., Maravel, A., Hao, J., Wang, J., Peters, J., and Bou Ammar, H. Hebo: Pushing the limits of sample-efficient hyperparameter optimisation. In *Journal of Artificial Intelligence Research*, 2022.

Das, A., Kong, W., Leach, A., Mathur, S., Sen, R., and Yu, R. Long-term forecasting with tide: Time-series dense encoder. *arXiv:2304.08424*, 2023a.

Das, A., Kong, W., Sen, R., and Zhou, Y. A decoder-only foundation model for time-series forecasting. *arXiv:2310.10688*, 2023b.

Dos Santos Diniz, F. J., Matos, S. N., Ueyama, J., Marcolino, L. S., Da Silva Luz, E. J., and Pessin, G. Uncertainty quantification in measuring ore mass flow rate with data-driven soft sensors. In *IEEE International Instrumentation and Measurement Technology Conference*, 2025.

Ekambararam, V., Jati, A., Dayama, P., Mukherjee, S., Nguyen, N. H., Gifford, W. M., Reddy, C., and Kalagnanam, J. Tiny time mixers (ttms): Fast pre-trained models for enhanced zero/few-shot forecasting of multivariate time series. In *Advances in Neural Information Processing Systems*, 2024.

Gao, S., Koker, T., Queen, O., Hartvigsen, T., Tsiligkaridis, T., and Zitnik, M. Units: A unified multi-task time series model. In *Advances in Neural Information Processing Systems*, 2024.

Godahewa, R. W., Bergmeir, C., Webb, G. I., Hyndman, R., and Montero-Manso, P. Monash time series forecasting archive. In *Neural Information Processing Systems Datasets and Benchmarks Track*, 2021.

Goswami, M., Szafer, K., Choudhry, A., Cai, Y., Li, S., and Dubrawski, A. MOMENT: A family of open time-series foundation models. In *International Conference on Machine Learning*, 2024.

Götz, L., Kollovieh, M., Günemann, S., and Schwinn, L. Efficient time series processing for transformers and state-space models through token merging. In *International Conference on Machine Learning*, 2025.

Hu, J., Qian, H., Han, S., Zhang, P., and Lu, Y. Light-activated virtual sensor array with machine learning for non-invasive diagnosis of coronary heart disease. In *Nano-Micro Letters*, 2024.

Hu, Y., Zhang, G., Liu, P., Lan, D., Li, N., Cheng, D., Dai, T., Xia, S.-T., and Pan, S. Timefilter: Patch-specific spatial-temporal graph filtration for time series forecasting. In *International Conference on Machine Learning*, 2025.

ISO 11898. Road vehicles - Interchange of digital information - Controller area network (CAN) for high-speed communication, 1993.

Kalyanasundaram, A., Sekaran, K. C., Stäuber, P., Lange, M., Utschick, W., and Botsch, M. Uncertainty-aware hybrid machine learning in virtual sensors for vehicle sideslip angle estimation. In *IEEE Intelligent Vehicles Symposium*, 2025.

Kingma, D. P. and Ba, J. L. Adam: A method for stochastic optimization. In *International Conference on Learning Representations*, 2015.

Lee, S., Park, T., and Lee, K. Partial channel dependence with channel masks for time series foundation models. *arXiv:2410.23222*, 2024.

Liu, Q., Fang, Y., Jiang, P., and Li, G. Dgcformer: Deep graph clustering transformer for multivariate time series forecasting. *arXiv:2405.08440*, 2024a.

Liu, Y., Zhang, H., Li, C., Huang, X., Wang, J., and Long, M. Timer: Generative pre-trained transformers are large time series models. In *International Conference on Machine Learning*, 2024b.

Liu, Y., Qin, G., Shi, Z., Chen, Z., Yang, C., Huang, X., Wang, J., and Long, M. Sundial: A family of highly capable time series foundation models. In *International Conference on Machine Learning*, 2025.

Nie, Y., Nguyen, N. H., Sinthong, P., and Kalagnanam, J. A time series is worth 64 words: Long-term forecasting with transformers. In *International Conference on Learning Representations*, 2023.

Patil, P., Varshney, A., Cherukumalli, M., Deshpande, H., Eun, L., Sahoo, D., and Chittar, N. MOPRHEUS: A foundation model for multivariate time series forecasting. In *1st ICML Workshop on Foundation Models for Structured Data*, 2025.

Qiu, X., Wu, X., Lin, Y., Guo, C., Hu, J., and Yang, B. Duet: Dual clustering enhanced multivariate time series forecasting. In *Association for Computing Machinery SIGKDD Conference on Knowledge Discovery and Data Mining*, 2025.

Rasul, K., Ashok, A., Williams, A. R., Ghonia, H., Bhagwatkar, R., Khorasani, A., Bayazi, M. J. D., Adamopoulos, G., Riachi, R., Hassen, N., Biloš, M., Garg, S., Schneider, A., Chapados, N., Drouin, A., Zantedeschi, V., Nevmyvaka, Y., and Rish, I. Lag-llama: Towards foundation models for probabilistic time series forecasting. *arXiv:2310.08278*, 2023.

Rumelhart, D. E., Hinton, G. E., and Williams, R. J. Learning internal representations by error propagation. 1985.

Srivastava, N., Hinton, G., Krizhevsky, A., Sutskever, I., and Salakhutdinov, R. Dropout: A simple way to prevent neural networks from overfitting. In *Journal of Machine Learning Research*, 2014.

Vaswani, A., Shazeer, N., Parmar, N., Uszkoreit, J., Jones, L., Gomez, A. N., Kaiser, L. u., and Polosukhin, I. Attention is all you need. In *Advances in Neural Information Processing Systems*, 2017.

von Bülow, F., Mentz, J., and Meisen, T. State of health forecasting of lithium-ion batteries applicable in real-world operational conditions. In *Journal of Energy Storage*, 2021.

Wang, L., Chessari, C., and Karpel, E. Inferential control of product quality attributes - application to food cooking extrusion process. In *Journal of Process Control*, 2001.

Wang, Y., Wu, H., Dong, J., Qin, G., Zhang, H., Liu, Y., Qiu, Y., Wang, J., and Long, M. Timexer: Empowering transformers for time series forecasting with exogenous variables. In *Advances in Neural Information Processing Systems*, 2024.

Williams, R. J. and Zipser, D. A learning algorithm for continually running fully recurrent neural networks. In *Neural computation*, 1989.

Woo, G., Liu, C., Kumar, A., Xiong, C., Savarese, S., and Sahoo, D. Unified training of universal time series forecasting transformers. *arXiv:2402.02592*, 2024.

Ziaukas, Z., Busch, A., and Wielitzka, M. Estimation of vehicle side-slip angle at varying road friction coefficients using a recurrent artificial neural network. In *IEEE Conference on Control Technology and Applications*, 2021.

A. Experiments

In this section, we provide additional information about our experimental settings and resources.

Datasets Throughout our experiments, we utilize Traffic as a standard benchmark dataset and a CAN bus dataset for evaluating our architecture in more complex and realistic deployment scenarios. The Traffic dataset measures the road occupancy at 862 locations in the San Francisco Bay Area. It utilizes identical sensors and captures them once every hour. Our large-scale CAN bus dataset records 1713 time series within a modern electric vehicle. It consists of continuous sensor measurements, categorical states, and event-based signals, in 100 ms granularity. Here, each signal has a distinct and interpretable purpose. While time series in the Traffic dataset share a similar daily and weekly periodic structure, e.g., due to work traffic, signal interactions in our CAN bus dataset are substantially more complex and diverse. We visualize these different characteristics in figure 7.

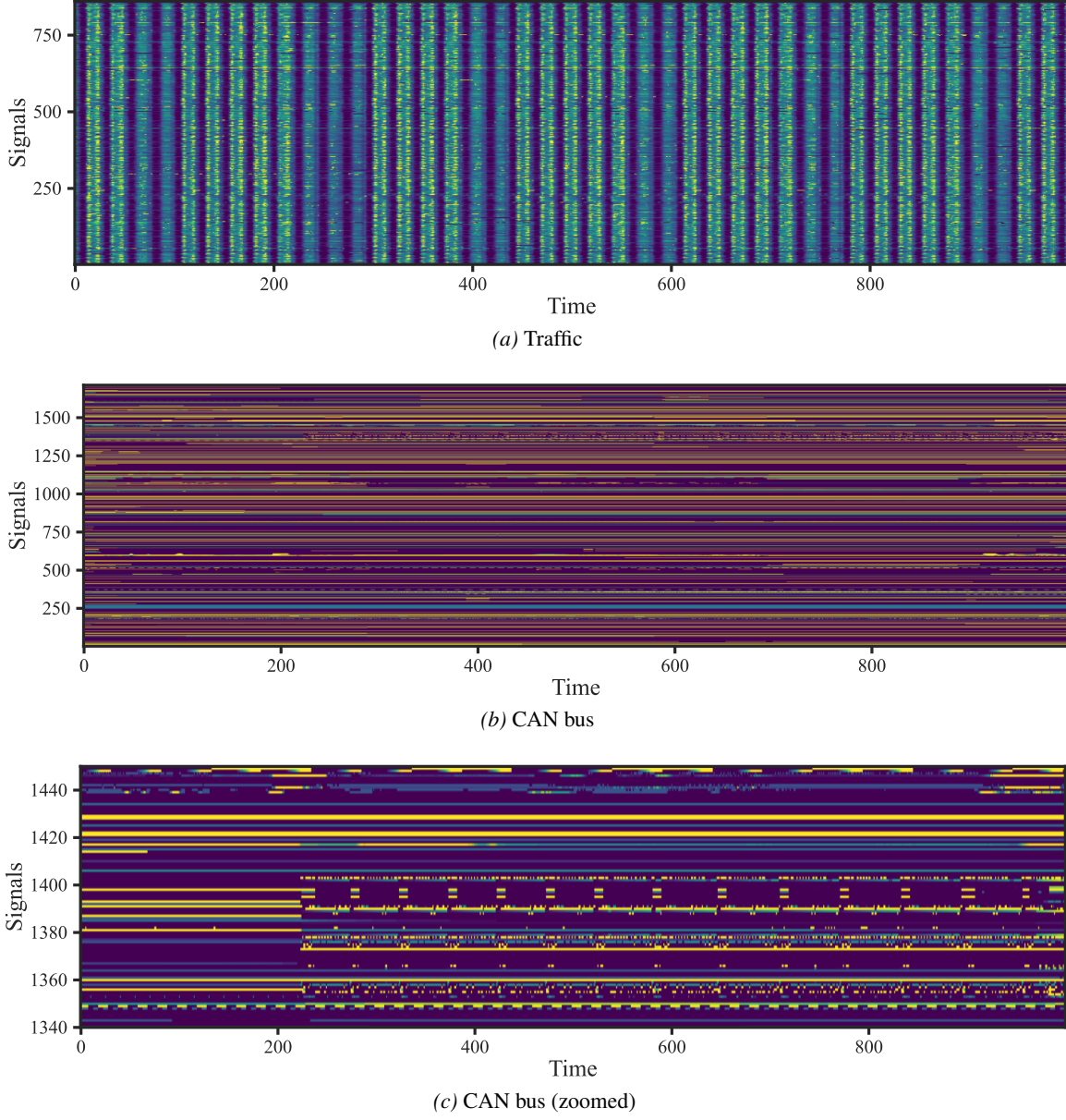


Figure 7. Signals on the Traffic and the CAN bus dataset show different temporal characteristics.

Virtual sensors We chose our $N = 16$ virtual sensors \mathcal{Z}' randomly for the Traffic dataset, including variate IDs $\{74, 88, 113, 173, 280, 311, 312, 352, 355, 478, 539, 646, 650, 715, 775, 776\}$, as all signals present the same quantity. For the CAN bus dataset with distinct signals, we hand-pick interesting virtual sensor tasks with clear intuitive interpretations according to table 4.

Table 4. Virtual sensors for the CAN bus dataset, which is recorded with an Audi e-tron electric vehicle.

Quantity	j
Battery	
Battery voltage	1
Battery current	2
Battery temperature	3
Battery coolant outflow temperature	4
Inverter temperature	5
Engine	
Engine 1 torque	6
Engine 1 voltage	7
Engine 1 current	8
Engine 1 power loss	9
Engine 1 temperature	10
Engine 1 rotor temperature	11
Engine 1 coolant intake temperature	12
Engine 1 coolant flow rate	13
Vehicle	
Wheel speed (rear, left)	14
Chassis ground clearance (rear, left)	15
Air condition power	16

Hyperparameters In preliminary experiments, we find promising hyperparameters which we list in table 5. We keep these architectural hyperparameters constant throughout our work to ensure a fair and isolated comparison of baselines with models with our proposed mechanisms. For all reported results and their underlying models, we conduct an extensive hyperparameter search over optimizer-related parameters, including the learning rate, using HEBO (Cowen-Rivers et al., 2022). This way we train competitive models that are robust to varying training dynamics.

Table 5. Hyperparameters for training our models. We denote sets as $\{\dots\}$ and continuous search spaces as $[\dots]$.

Hyperparameter	Value
Architectural	
Patch length	$p = 32$
Transformer layers	$L = 4$
Attention heads	4
Token dimension	$d = 512$
Multi-layer perceptron hidden dimension	512
Activation	ReLU
Optimizer-related	
Seed	2025
Optimizer	Adam (Kingma & Ba, 2015)
Learning rate	$[10^{-6}, 10^{-4}]$
Learning rate warm-up iterations	$\{0, 2, 4\}$
Learning rate warm-up start factor	$[0.3, 0.9]$
Learning rate decay step size	$\{0, 1\}$
Learning rate decay gamma	$[0.96, 0.99]$
Dropout	$[0.0, 0.2]$
Batch size	32
Epochs	80
Early stopping patience	9
Loss	MSE

Reproducibility of measurements For our main experiments, we report efficiency gains in end-to-end inference time and memory, as these real-world measurements are of most practical interest. For runtime profiling, we use the same Nvidia A6000 GPU with 2 warm-up and 2 measurement runs per batch to achieve inference time standard deviations $< 2\%$. Regarding memory allocation, we report dynamic CUDA peak memory, which is a deterministic quantity. Static memory offsets from model parameters are irrelevant in our evaluations as we explore models of similar size throughout our paper.

For more in-depth evaluations, we additionally utilize sparsity as a hardware-independent efficiency measure. We explore relations between inference time, memory, and sparsity in [appendix B.6](#).

Computational effort We utilize over 43 500 compute hours on Nvidia H100 GPUs to train our foundation models. To improve training efficiency, we employ 16-bit mixed-precision strategies with `bfloat16` data types. We estimate the computational effort to reproduce our experiments in [table 6](#). Please note that we reuse previously trained models in many of our experiments.

Table 6. Computational effort to reproduce our experiments.

Experiment	GPU hours	Models trained
Main experiment	9384	1272
Main experiment – individual baselines	7392	1078
Main experiment – unified baselines	1044	492
Different MSE efficiency trade-offs for variable test-time computation	4242	160
Scaling to hundreds of virtual sensors	8776	660
Explainability of virtual sensors – Quantitative assessment	786	42
Explainability of virtual sensors – Synthetic data	1	1
Efficient training strategies – Training virtual sensors simultaneously	7920	560
Efficient training strategies – Teacher forcing	3964	36

B. Results

Here, we show additional experiments and results.

B.1. Different MSE efficiency trade-offs for variable test-time computation

In [figure 8](#) we provide complete results of our investigations of different MSE efficiency trade-offs on the Traffic and the CAN bus dataset.

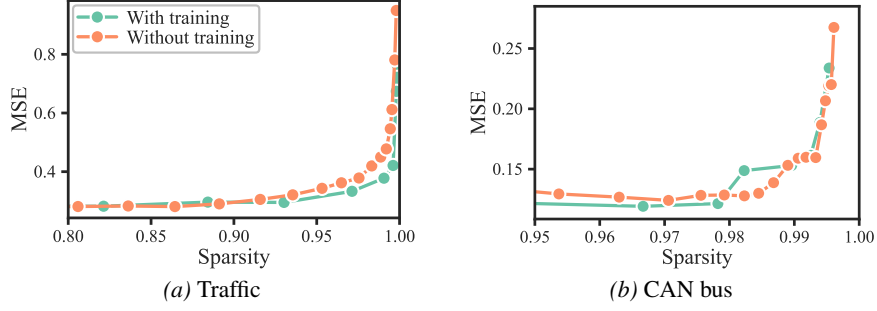


Figure 8. Varying our signal importance threshold r'_{thres} during training or inference generates smooth trade-offs between input set sparsity and MSE on the Traffic and the CAN bus dataset.

B.2. Sensor selection maximizes efficiency without affecting predictive quality

Here, we demonstrate efficiency gains through our sensor selection mechanism on the Traffic and the CAN bus dataset in [figure 9](#).

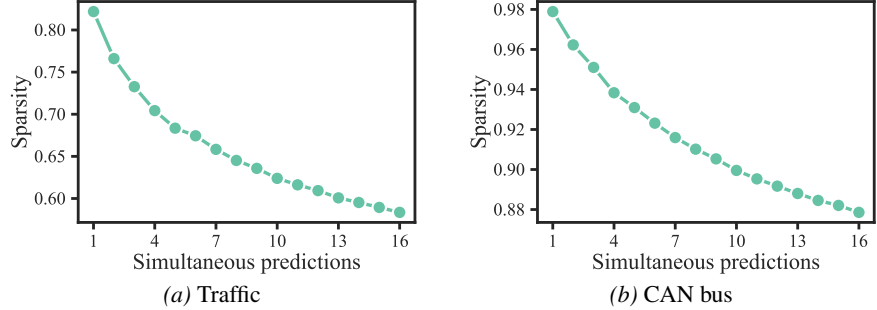


Figure 9. Sparsity increases as fewer virtual sensors are predicted simultaneously through our sensor selection mechanism. Results are shown for the Traffic and the CAN bus dataset.

B.3. Efficient training strategies – Training virtual sensors simultaneously

[Figure 10](#) shows complete results for training multiple virtual sensors simultaneously on the Traffic and the CAN bus dataset.

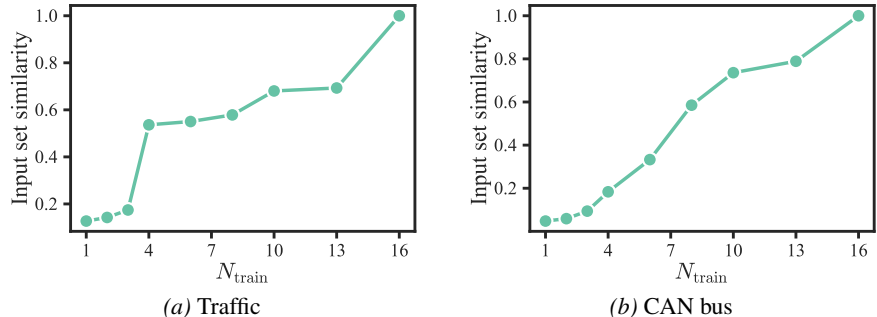


Figure 10. Learning different numbers of virtual sensors N_{train} in a single training iteration influences the similarity of their input signal sets on the Traffic and the CAN bus dataset.

B.4. Learning relevant input signals

Our architecture learns individual input signal sets for each virtual sensor as described in sections 3.3 and 5.2. Here, we provide further insights into the training process. Throughout training, our signal relevance vectors \mathcal{R}' learn signal importance from attention gradients, becoming more diverse as training proceeds in figures 11a to 11f. Next, we distinguish between important and unimportant signals using a threshold r'_{thres} to sparsify our signal relevance vectors in figures 11g and 11h, effectively disregarding irrelevant input signals. This finally results in individual input signal sets $\mathcal{Z}_j \subseteq \mathcal{Z}$ for every virtual sensor in figure 12. On the CAN bus dataset, where each signal has a distinct and interpretable purpose, this offers novel explainability of the virtual sensors. Assessment from domain experts further validates meaningful signal selections.

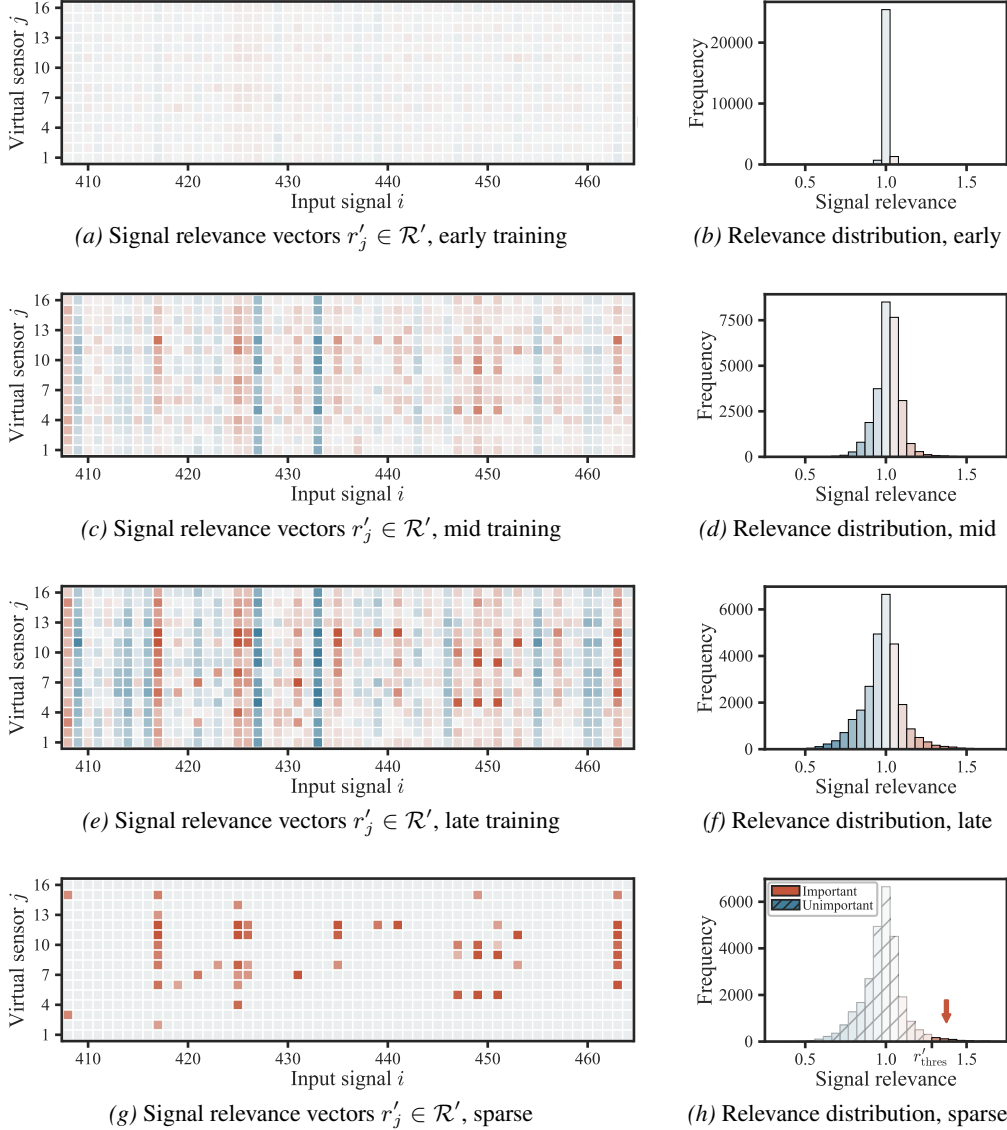


Figure 11. **(a-f)** Signal relevance vectors evolve during training on the CAN bus dataset. **(g,h)** We sparsify signal relevance using a threshold r'_{thres} to exclude irrelevant signals, keeping only important ones (arrow).

Battery voltage ($j = 1$)	Battery current ($j = 2$)	Battery temp. ($j = 3$)
<ul style="list-style-type: none"> Battery charge voltage Battery charge current Battery open loop voltage Engine 2 voltage ... 	<ul style="list-style-type: none"> Battery charge current Engine 1 mode (on, idle, off) Vehicle velocity Vehicle heating demand ... 	<ul style="list-style-type: none"> Battery coolant in temp. Vehicle heating demand Vehicle cooling demand Vehicle velocity ...
Battery coolant out temp. ($j = 4$)	Inverter temp. ($j = 5$)	Engine 1 torque ($j = 6$)
<ul style="list-style-type: none"> Battery coolant in temp. Barerry coolant flow rate Ambient temp. Vehicle velocity ... 	<ul style="list-style-type: none"> Engine 2 temp. Battery coolant in temp. Ambient temp. Vehicle velocity ... 	<ul style="list-style-type: none"> Engine 1 speed Accelerator pedal position Vehicle velocity Driving direction ...
Engine 1 voltage ($j = 7$)	Engine 1 current ($j = 8$)	Engine 1 power loss ($j = 9$)
<ul style="list-style-type: none"> Engine 2 voltage Battery open loop voltage Battery discharge voltage Battery charge voltage ... 	<ul style="list-style-type: none"> Accelerator pedal position Vehicle velocity Engine 1 speed Engine 2 power loss ... 	<ul style="list-style-type: none"> Engine 2 power loss Engine 1 speed Accelerator pedal position Brake pedal position ...
Engine 1 temp. ($j = 10$)	Engine 1 rotor temp. ($j = 11$)	Engine 1 coolant in temp. ($j = 12$)
<ul style="list-style-type: none"> Engine 2 temp. Engine 2 rotor temp. Engine 1 speed Battery coolant in temp. ... 	<ul style="list-style-type: none"> Engine 2 rotor temp. Engine 2 temp. Engine 1 speed Battery coolant in temp. ... 	<ul style="list-style-type: none"> Battery coolant in temp. Evaporator temp. Evaporator power Ambient temp. ...
Engine 1 coolant flow rate ($j = 13$)	Wheel speed (rear, left) ($j = 14$)	Ground clear. (rear, left) ($j = 15$)
<ul style="list-style-type: none"> Vehicle cooling demand Vehicle heating demand Engine 2 coolant flow rate Engine 1 speed ... 	<ul style="list-style-type: none"> Wheel speed (rear, right) Engine 1 speed Vehicle velocity Driving direction ... 	<ul style="list-style-type: none"> Ground clear. (rear, right) Driving mode (eco, sport, comfort) Vehicle velocity Driving direction ...
Air condition power ($j = 16$)		
<ul style="list-style-type: none"> Vehicle cooling demand Vehicle heating demand Vehicle desired temp. Fan speed ... 		

Figure 12. Individual input signal sets $\mathcal{Z}_j \subseteq \mathcal{Z}$ for each virtual sensor j for the CAN bus dataset, learned by our model. For clarity, we list only 4 input signals, while virtual sensors use 38 on average. Further, heating and cooling demand signals relate to the vehicle’s interior but also to drivetrain components such as the battery and engine. (See table 4 for non-abbreviated virtual sensor names.)

B.5. Interactions

There are complex interactions between training efficiency, inference efficiency, and prediction quality, which we explore here in detail. Increasing N_{train} to learn multiple virtual sensors at a time improves training efficiency. It also leads to more similar input sets $\mathcal{Z}_j \subseteq \mathcal{Z}$ for the virtual sensors (see figure 6). This has two major effects during inference. First, for a fixed prediction quality, the sensor's input sets need to be larger and less sparse as they are less specialized (see figure 13a). This reduces peak efficiency when predicting virtual sensors individually (figure 13b). Second, when forecasting multiple virtual sensors at a time, more similar input sets lead to graceful scaling as in figure 13b. Here, synergies among input sets benefit efficiency.

For the Traffic dataset, peak inference efficiency for individual virtual sensors is $3.8 \times$ higher for runtime and $5.2 \times$ for memory compared to constant scaling behavior for multiple virtual sensors. Generally, we suggest training multiple virtual sensors simultaneously for multi-sensor inference use cases, while learning single virtual sensors at a time for peak inference efficiency of individual virtual sensors. Note that quantitative efficiency gains are strongly dependent on the choice of virtual sensors and the dataset.

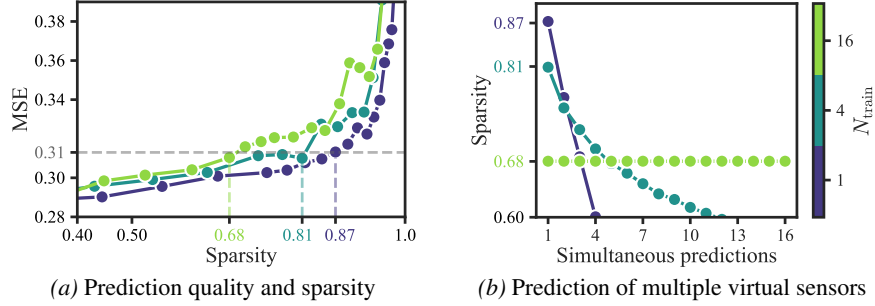


Figure 13. Learning different numbers of virtual sensors N_{train} in every training iteration influences (a) tradeoffs between predictive quality and sparsity and (b) inference efficiency when predicting multiple virtual sensors simultaneously on the Traffic dataset.

B.6. Real-world efficiency gains through sparsity

In our main experiments, we report efficiency gains in inference time and memory, which are of high practical relevance. For more in-depth analysis, we also report sparsity. Here, we explore relations between sparsity, runtime, and memory allocation in detail.

Our architecture employs sparsity in a structured way by reducing the transformer's input tokens s to a minimum. It focuses only on relevant input signals for a requested set of virtual sensors as described in sections 3.2, 3.3, 5.2 and 5.3. We profile our architecture with varying sparsity values in the following. Remarkably, our structured sparsity directly yields real-world savings in computation time and memory over several orders of magnitude, as our results in figure 14 show. For low sparsity values, the attention operation with quadratic complexity is most dominant, while the transformer's multi-layer perceptron with linear complexity is the limiting operation in high-sparsity regimes.

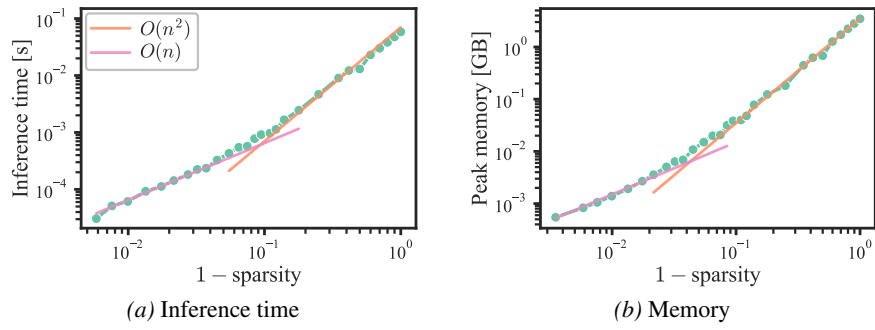


Figure 14. Structured sparsity induces savings in inference time and dynamic CUDA peak memory. Note that we visualize $1 - \text{sparsity}$ on logarithmic axes. Therefore, quadratic and linear complexities transform into linear functions with slopes of 2 and 1, respectively.

B.7. Visualization of virtual sensor predictions

In this section, we illustrate predictions of our virtual sensor foundation model on the Traffic dataset. In contrast to standard time series forecasting literature (Nie et al., 2023), our architecture does not have a fixed context horizon. Instead, it forecasts virtual sensors $p = 32$ time steps from other measurement signals, starting from empty prototype tokens. In the following autoregressive cycles, our model also utilizes its past virtual sensor predictions. Over time, past context grows, mimicking practical deployment scenarios of virtual sensors. Our visualizations in figure 15 demonstrate that our architecture successfully predicts initial virtual sensor values from empty prototypes. Subsequent autoregressive cycles do not show error accumulation and predicted patches connect smoothly. Finally, our sensor selection mechanism successfully switches between multiple virtual sensors with different temporal characteristics, measuring traffic flow at different locations in San Francisco. All this visual evidence aligns with our previous results, demonstrating the flexibility of our approach.

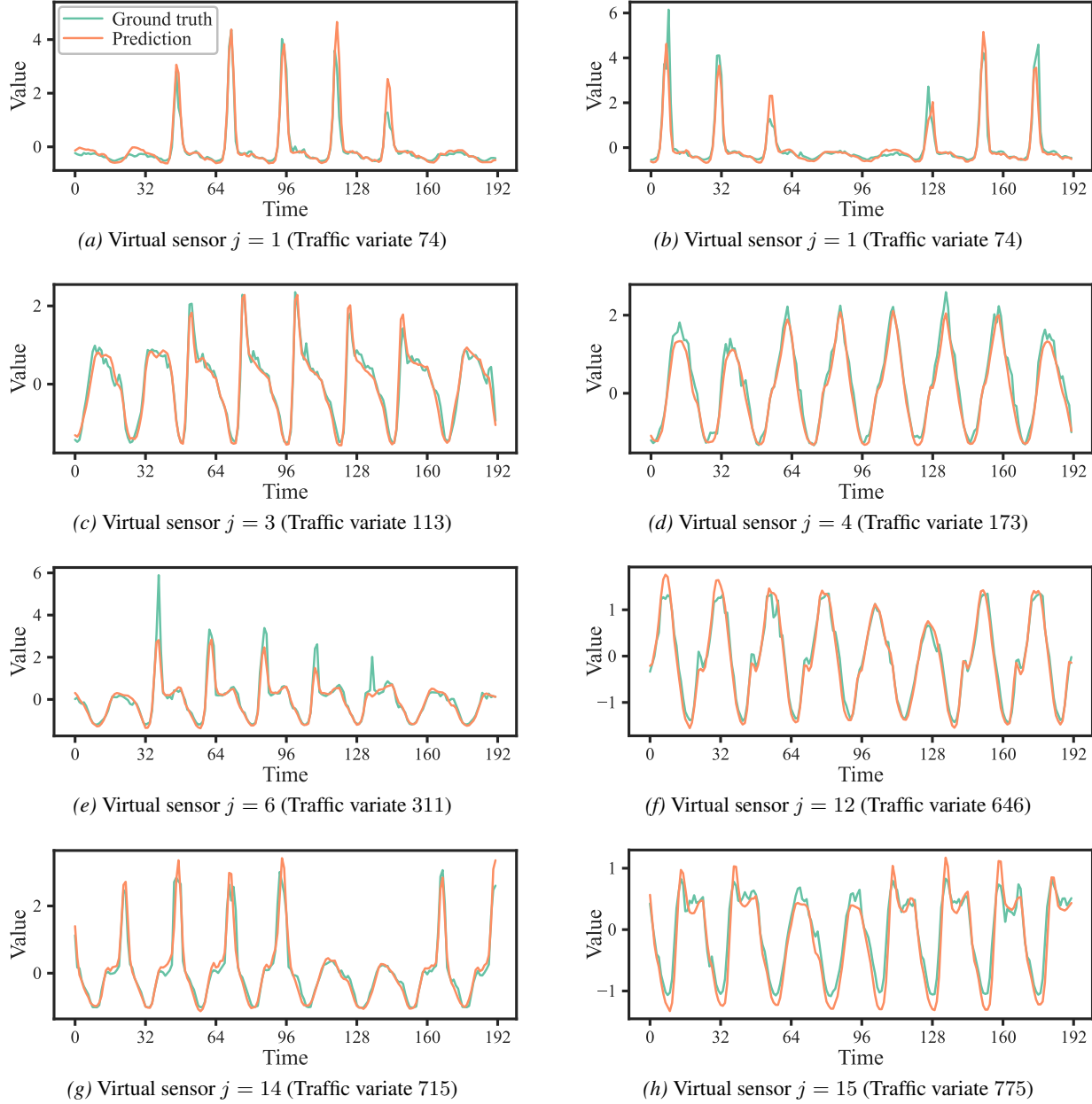


Figure 15. Virtual sensor predictions on the Traffic dataset. Our sensor selection mechanism successfully switches between virtual sensors with different temporal patterns.